MODELING URBAN CARBON DIOXIDE USING LIGHT-RAIL MEASUREMENTS AND THE MODIFIED STOCHASTIC TIME-INVERTED LAGRANGIAN TRANSPORT MODEL (STILT-R VERSION 2)

by

Benjamin Fasoli

A thesis submitted to the faculty of
The University of Utah
in partial fulfillment of the requirements for the degree of

Master of Science

Department of Atmospheric Sciences

The University of Utah

December 2017

The University of Utah Graduate School

STATEMENT OF THESIS APPROVAL

The thesis of **Benjamin Fasoli**

has been approved by the following supervisory committee members:

John Chun-Han Lin	, Chair	**August 7, 2017** Date Approved
David R. Bowling	, Member	**August 7, 2017** Date Approved
John D. Horel	, Member	**August 7, 2017** Date Approved

and by **Kevin D. Perry** , Chair/Dean of

the Department/College/School of **Atmospheric Sciences**

and by David B. Kieda, Dean of The Graduate School.

ABSTRACT

The Stochastic Time-Inverted Lagrangian Transport (STILT) model is comprised of a compiled Fortran executable that carries out advection and dispersion calculations as well as a higher level code layer for simulation control and user interaction, written in the open source data analysis language R. We introduce modifications to the STILT-R codebase with the aim to improve the model's applicability to fine-scale trace gas measurement approaches. The changes facilitate placement of spatially distributed receptors and provide high level methods for single and multinode parallelism. We present a kernel density estimator to calculate influence footprints and demonstrate improvements over previous methods. This framework provides a central source repository to reduce code fragmentation between STILT user groups as well as a systematic, well-documented workflow for users. We apply the modified STILT to light-rail measurements in Salt Lake City, UT and discuss how results from our analyses can inform future fine-scale measurement approaches and modeling efforts.

TABLE OF CONTENTS

LIST OF FIGURES

Figures

ACKNOWLEDGMENTS

I would like to thank my advisor, John C. Lin, as well as my family, friends, and loved ones for their continued support.

CHAPTER 1

INTRODUCTION

The atmospheric carbon budget is governed by sources and sinks, which are dominated by the interplay between anthropogenic emissions and uptake by oceans, the terrestrial biosphere, and the atmosphere. Anthropogenic emissions have spiked with human use of fossil fuels since the industrial revolution. Direct measurements have shown that human activity is driving these sources and sinks out of balance (Raupach and Canadell, 2010; U.S. EPA, 2016) resulting in rapidly increasing atmospheric carbon. Together, carbon dioxide (CO_2) and methane (CH_4) account for over 90% of U.S. anthropogenic greenhouse gas emissions (U.S. EPA, 2016) and are the focus of the majority of greenhouse gas climate research, as well as this work.

CO_2 represents the primary contribution to anthropogenic climate change. Atmospheric CO_2 mole fraction has increased by more than 40% since pre-industrial times largely due to emissions caused by fossil fuel consumption (Raupach and Canadell, 2010). CO_2 is a potent greenhouse gas because molecules can remain in the atmosphere for hundreds of years and its absorption spectrum lies close to the wavelength of peak emission from the Earth's surface (Wallace and Hobbs, 2006). Further, localized CO_2 emissions in isolation increase local ozone and particulate matter and may result in 300-1000 premature deaths per year in the U.S. alone (Jacobson, 2010). In this way, CO_2

emissions and fossil fuel use are a problem for global environmental change as well as human health at the county and city scale.

While CH_4 has a residence time in the atmosphere of only 12 years (US EPA, 2015) and exists at ambient mole fractions that are two orders of magnitude smaller than that of CO_2, CH_4 molecules are far more efficient at trapping outgoing radiation. On a 100-yr timescale, a CH_4 molecule will have at least 25 times the greenhouse effect of a molecule of CO_2 (US EPA, 2015). Further, global atmospheric CH_4 concentrations are rising at a fractional rate exceeding that of CO_2 and have increased by about 150% over the past two centuries (Wolff, 2011) following a long-term period of relative stability (Meure et al., 2006). As a global annual mean, over 60% of total CH_4 emissions are associated with human activities. The consumption of fossil fuels, including natural gas and petroleum systems, are the largest CH_4 source in the U.S., followed by the agriculture industry and waste decomposition (US EPA, 2015). While emissions inventory estimates show no discernible trend in the U.S. anthropogenic CH_4 emissions since 2002, satellite retrievals and surface measurements suggest that U.S. CH_4 emissions have increased by more than 30% during this period (Turner et al., 2016). The natural gas supply chain accounts for the majority of CH_4 emissions in the 2012 Environmental Protection Agency Greenhouse Gas Inventory, with 90% of emissions attributed to compressors and exhaust from engines and turbines (Marchese et al., 2015).

1.1 Emissions from urban systems

Carbon emissions from cities represent the single largest human contribution to climate change (Duren and Miller, 2012; Gurney et al., 2015) and will become

increasingly important as urban population growth exceeds changes in rural populations. Between 1980 and 2010, the U.S. urban population grew by 81 million people while rural populations declined slightly (Gately et al., 2015). Future projections show that urban land area is expected to increase by 1.2 million km^2 by 2030, nearly tripling the urban land cover in 2000 (Seto et al., 2012). However, we have only recently begun to study these emissions at the fine spatial and temporal scales needed to inform policy makers about where, when, and how emissions could be reduced most effectively. Studies have shown main roads and large buildings are the largest urban emitters of CO_2 (Gurney et al., 2015) while patterns in CH_4 emissions are more spatially uniform with few large point sources, such as leaks in natural gas infrastructure (McKain et al., 2015). Improving our knowledge of CO_2 and CH_4 mole fractions on the scale at which they are emitted is crucial to understand the impacts of urban emissions.

Several factors influence localized CO_2 flux, including but not limited to proximity to urban centers, roads, industrial sources, and vegetation. A 2002 study (Wentz et al., 2002) applied regression-based analyses to estimate surfaces of CO_2 mole fraction in Phoenix, Arizona. Findings show that dominant patterns in the spatial structure of CO_2 vary depending on the time of day and day of week. Bulk estimates of urban CO_2 emissions have been calculated using various methods (Mays et al., 2009; Christen, 2014; Turnbull et al., 2015) and long-term studies show significant increases in ambient CO_2 mole fraction in and around urban areas over time (Newman et al., 2008; Gurney et al., 2009). Several studies have found that CO_2 fluxes in and around urban areas are largely impacted by traffic and natural gas home heating (Kennedy et al., 2009) as well as land cover, climate, and time of year (Ramamurthy and Pardyjak, 2011).

However, significant heterogeneities exist across the urban to rural gradient in how, where, and when these CO_2 fluxes occur (Briber et al., 2013). The pattern of higher CO_2 mole fraction in urban areas relative to the surrounding rural areas is characteristic of urban CO_2 "domes" (Idso et al., 2001; Pataki et al., 2007), where considerable city-center concentration enhancements are observed relative to the surrounding area. These urban CO_2 domes result primarily from the burning of fossil fuels (Idso et al., 2001) and may increase the local ozone and particulate matter directly impacting the health of those living in urban areas (Jacobson, 2010).

Studies have largely attributed the rise in global atmospheric CH_4 to the production, distribution, and consumption of fossil fuels, much of which occurs in and around urban areas. Urban CH_4 source attribution studies in Boston and the Los Angeles Basin have used mobile van-based laboratories to simultaneously measure atmospheric ethane (C_2H_6) and CH_4. These data were compared to direct measurement of the ethane-to-methane ratios of known sources and coupled with atmospheric transport models. This analysis indicated that natural gas accounts for 60-100% of methane emissions depending on season (McKain et al., 2015) and remains the dominant source of CH_4 in regionally integrated air (Hopkins et al., 2016). Similarly, a 2012 Boston study measured $\delta 13CH_4$ isotopic compositions of urban CH_4 leaks and demonstrated that the $\delta 13CH_4$ signatures (mean = −42.8‰ ± 1.5‰) strongly indicate fossil fuels are the dominant source for most leaks (Phillips et al., 2013).

Emissions inventories are beginning to merge atmospheric measurements with estimations of carbon emissions from fuel usage, traffic data, building information, and human activity (Mays et al., 2009; Gurney et al., 2012). To resolve surface level

emissions, transport models need to assimilate abundant ground- and satellite-based atmospheric concentration and meteorological data. Collecting and analyzing data for these studies is costly and has only been attempted for a few cities around the world (Gurney et al., 2015). Salt Lake City possesses uniquely dense measurement networks and has been the subject of one such study (Gurney et al., 2012).

1.2 Observation techniques

Surface-level measurements provide novel opportunities to better quantify emissions (Duren and Miller, 2012; Christen, 2014), evaluate population exposure to pollution (Jacobson, 2010; Clark et al., 2014), and validate both inventories and model predictions. However, very few measurements are made at a spatial scale capable of examining finer scale patterns of trace gases and pollutant concentrations in urban areas. Trace gases and species directly attributable to poor air quality are traditionally monitored using stationary (in-situ) observation sites, thereby limiting the collected data to a single point in space that may have limitations in characterizing the surrounding area.

Recent innovations in high-frequency trace gas analyzers enable their use on mobile platforms that provide direct observations of spatial concentration patterns. We have developed mobile platforms to complement stationary observation sites to better constrain the heterogeneity and complexities of urban emissions. High-frequency trace gas and criteria pollutant measurements operate continuously on a Salt Lake Valley-based light-rail train (TRAX) and semicontinuously during research campaigns using a van-based mobile laboratory (known as the Nerdmobile). These mobile data quantify changes in trace gas concentrations at a scale smaller than a single city block and can be

combined with stationary observations to improve understanding of fine-scale urban trace gas and pollutant concentrations (Figure 1.1).

1.2.1 TRAX light-rail train

Light-rail trains offer several advantages over other trace gas measurement techniques including repeated transects along the same path, low operating costs, and zero emissions from the train that could impact measurements. TRAX has performed regular hour-long transects across the Salt Lake Valley since December, 2014 on one of two different routes resulting in pseudo-continuous concentration lines. The red line travels a southwest to northeast transect between the Daybreak and University of Utah CO_2 monitoring stations. The green line travels a U-shaped transect from the Salt Lake International Airport (northwest) to downtown Salt Lake City, then southwest into West Valley City.

TRAX hosts a Los Gatos Research (LGR) Ultraportable Greenhouse Gas Analyzer (CO_2, CH_4), a 2B Technologies model 205 (O_3), Met One E-Sampler ($PM_{2.5}$), a suite of meteorological measurements including temperature, pressure, and relative humidity, and a GRIMM model 1.109 for relevant studies ($PM_{2.5}$, particle size distribution). Instruments are interfaced to a central single-board Linux computer that controls instruments and calibration systems and continuously logs over 70 simultaneously measured variables. These systems calibrate the LGR hourly against a single reference gas, which is sufficient to qualify the measurements across a wide range of concentrations due to the LGR's exceptional linearity in both CO_2 and CH_4 space. Other measurements are calibrated on a seasonal basis. Data are processed and calibrated

on a remote server and measurements are made available in real-time via the web (air.utah.edu).

While each individual transect provides limited information about spatial concentration distributions measurements occur at different times, long-term spatial and temporal averaging of 1,500 red line and 1,300 green line transects reveal dominant patterns across the urban landscape. In agreement with the urban CO_2 dome, data show the highest mole fractions in the urban core, decreasing as the train moves further away from the I-15 corridor. The lowest observations frequently occur furthest from downtown Salt Lake City near the Daybreak observation site, the University of Utah, and the Salt Lake International Airport.

1.2.2 $SLCCO_2$ measurement sites

The Salt Lake City CO_2 ($SLCCO_2$) network, consisting of six closed-path infrared gas analyzers, characterizes CO_2 mole fraction across the Salt Lake Valley (Figure 1.1). Rose Park (1), Sugarhouse (2), and Murray (3) are largely representative of Salt Lake City's urban corridor that closely follows interstate highway 15. The observed patterns (Figure 1.2) are most directly attributed to local emissions, as can be seen during times of peak emissions such as rush hour traffic. The University of Utah (4), located just outside of downtown Salt Lake City and 500 feet above the valley floor, is representative of the surrounding suburban areas. While none of the measurements represent a true atmospheric background signal, Daybreak (5), located west of much of the urban development and 500 feet above the valley floor, and Suncrest (6), located in the southeast corner of the valley and 1800 feet above the valley floor, are both located in

more rural areas and generally capture lower CO_2 concentrations than sites closer to downtown.

1.2.3 Nerdmobile mobile laboratory

Despite the many advantages afforded by using TRAX and the stationary observation network for continuous data collection, both are limited in the spatial range of observations. The Nerdmobile enables data collection in areas lacking TRAX observations or traditional in-situ stations and can be deployed to answer specific research questions (Figure 1.3). This mobile laboratory hosts two Picarro CRDS (CO_2/CO, CO_2/CH_4), a 2B Technologies 205 (O_3), a 2B Technologies model 410/401 (NO_x), a GRIMM model 1.109 ($PM_{2.5}$, particle size distributions), a flask filling system used for isotopic analyses, and a suite of meteorological measurements including temperature, pressure, relative humidity, and wind speed and direction. Additionally, the Nerdmobile is capable of adapting the measured species to better suit the needs of research studies by hosting short-term instrumentation.

Instruments are interfaced to a central Linux computer that controls measurement and calibration systems and continuously logs over 60 simultaneously measured variables. This system also hosts a wireless dashboard to a designated iPad (Figure 1.3), allowing the operator to monitor incoming measurements and diagnostics in real-time, control onboard valves and pumps, record geotagged notes and flask observations, and access in-depth documentation for diagnosing problems with instruments or control systems. Data are processed and calibrated on a remote server and measurements are made available in real-time via the web (air.utah.edu).

1.3 Modeling emissions

1.3.1 Hestia inventory

Emissions inventories have vastly improved in their accuracy and their temporal and spatial resolutions in recent years (Gurney et al., 2009). Salt Lake City is one of four cities in the world for which the Hestia anthropogenic emissions inventory has been produced (Gurney et al., 2012). Hestia was developed to improve our understanding of the exchange of carbon between the land and atmosphere at a fine spatial and temporal scale. The model takes a bottom-up approach to estimate anthropogenic carbon flux by characterizing emissions at the scale of individual buildings and roadways. Furthermore, emissions are disaggregated into individual economic sectors, including Non-point Residential and Commercial Buildings, Industrial Non-point Buildings, Industrial, Commercial, and Energy Production Point Sources, and Transportation. These emissions vary over space and time and generally depend on factors such as location, day of week, time of day, and energy use.

1.3.2 Stochastic Time-Inverted Lagrangian Transport (STILT) model

While spatial and temporal averaging of measurements can reveal long-term patterns in concentrations along the mobile transect routes, coupling the data with atmospheric transport models enables the inversion of measured concentrations to estimate surface fluxes. The Stochastic Time-Inverted Lagrangian Transport (STILT) model simulates transport by releasing an ensemble of particles, linearly interpolating meteorological fields to the sub-grid scale, and following the particle trajectories back in time. This method allows the determination of surface fluxes from background

atmospheric concentrations in the form of STILT footprints, which represent the fractional contributions of spatially distributed sources and sinks on observed concentrations (Lin et al., 2003). This research applies the STILT model in two previously unutilized capacities. First, this research couples STILT with the High Resolution Rapid Refresh (HRRR) wind fields for the Salt Lake Valley. The HRRR is a NOAA operational model that provides hourly fields at a 3-km horizontal resolution (Sun et al., 2014). STILT simulations are often coupled with the Weather Research and Forecasting (WRF) model which helps to reduce transport errors in top-down estimates of terrestrial greenhouse gas fluxes (Nehrkorn et al., 2010). However, this method can be very computationally expensive to produce the WRF wind fields that drive STILT particle dispersion. Utilization of the HRRR model, for which the model fields are available for the U.S. beginning in 2015, eliminates the dependency on WRF simulations and reduce computational costs. Second, we apply STILT to mobile measurements made by the TRAX light-rail train, discuss the model's applicability to fine-scale spatial measurements, and explore how results can inform future modeling and measurement efforts.

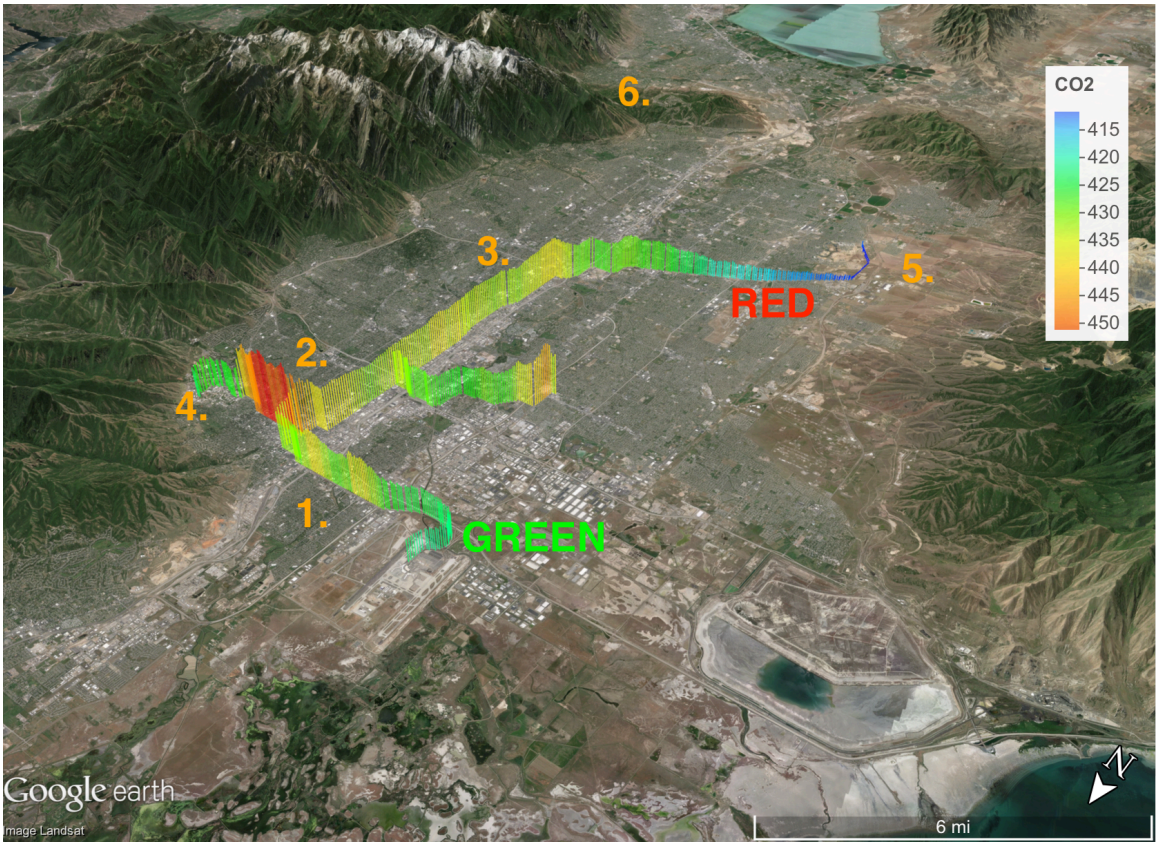

Figure 1.1. Spatially distributed measurement sites in the Salt Lake Valley: 1. Rose Park, 2. Sugarhouse, 3. Murray, 4. University of Utah, 5. Daybreak, 6. Suncrest. The colored vertical bars depict the spatiotemporal average CO_2 mole fraction across the urban landscape as seen by the TRAX train on the red and green light-rail routes for January to December 2016. These data clearly show the urban CO_2 dome surrounding downtown Salt Lake City.

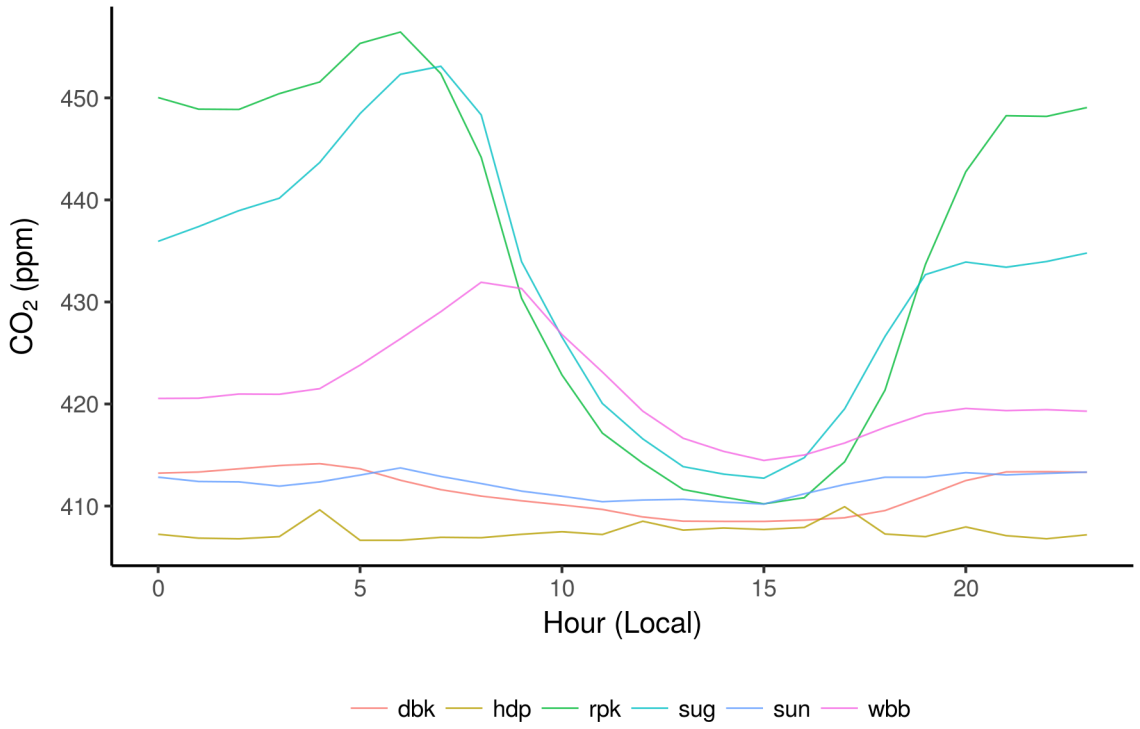

Figure 1.2. Average daily CO_2 mole fraction by hour for each SLCCO$_2$ measurement site for January 2016 to December 2016, with the nearby Hidden Peak background site shown for reference (http://raccoon.ucar.edu).

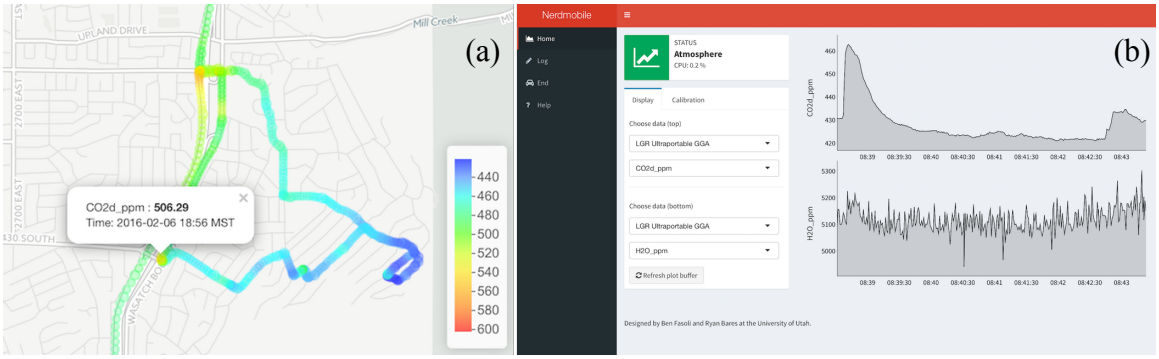

Figure 1.3. Nerdmobile measurements (a) show significant changes in CO_2 concentrations while traveling east toward higher elevations. Data and diagnostics can be accessed in real-time by the operator through an iPad-based measurement dashboard (b).

CHAPTER 2

MODELING SPATIALLY DISTRIBUTED RECEPTORS WITH THE STOCHASTIC TIME-INVERTED LAGRANGIAN TRANSPORT (STILT) MODEL: UPDATES TO THE R INTERFACE OF STILT (STILT-R VERSION 2)

2.1 Introduction

Atmospheric measurements (Duren and Miller, 2012; McKain et al., 2012) as well as fuel consumption statistics, traffic data, and building characteristics (Gurney et al., 2009, 2012) clearly indicate that fossil fuel consumption is concentrated in urban areas. Cities are the source of over 70% of global fossil-fuel carbon dioxide (CO_2) emissions (Hoornweg et al., 2011; Gurney et al., 2015), the largest anthropogenic forcing on climate change (Canadell et al., 2007). As governing bodies examine ways to address climate change, urban areas are appropriately the focus for emissions regulation. However, traditional strategies for measuring CO_2 mole fraction focus on quantifying regional scale averages. Implementing and verifying effective reduction policy requires understanding where, when, and how emissions occur at an intracity scale.

Novel measurement strategies and emissions inventories are striving toward spatial and temporal scales that resolve intracity trace gas concentrations. However,

traditional tools for interpreting these data were not designed for spatially distributed measurements such as trains, buses, and cars (Bush et al., 2015; Apte et al, 2017; Lee et al., 2017) or dense networks of inexpensive sensors (Shusterman et al., 2016; Turner et al., 2016). To make use of measurement advances, modeling approaches must adapt to finer scales and facilitate placement of spatially distributed receptors.

Lagrangian particle dispersion models (LPDMs) are popular tools for simulating atmospheric transport and dispersion. LPDMs transport an ensemble of theoretical particles using a mean trajectory scheme derived from meteorological model fields. Random turbulent motions are represented by a Markov process. This approach offers advantages over Eulerian methods by explicitly simulating transport trajectories and better representing atmospheric mixing, turbulent eddies, and convection. Particle motion can be simulated either forward in time from an emissions source or backward in time from a location of interest, referred to as the "receptor". The forward configuration is often used to simulate pollutant concentrations downstream from an emission source (Stohl et al., 2005) whereas backward simulations determine the source of observed emissions and estimate surface fluxes (McKain et al., 2012, 2015; Stein et al., 2015). As receptors are often greatly outnumbered by sources, significant computational savings are realized by applying STILT in the receptor-oriented configuration.

The STILT model couples Lagrangian particle dispersion with the mean advection scheme from the Hybrid Single-Particle Lagrangian Integrated Trajectory (HYSPLIT) model (Stein et al., 2015). STILT preserves time reversibility (Lin et al., 2003), enables quantitative evaluation of transport error (Lin and Gerbig, 2005), and is closely coupled with the commonly used Weather Research and Forecasting mesoscale

model (Nehrkorn et al., 2010), on which the state-of-the-science experimental High Resolution Rapid Refresh (HRRR) model is based (Sun et al., 2014). STILT is most commonly used to follow the backwards time evolution of a particle ensemble and calculate a receptor's footprint, a sensitivity matrix defining the upstream area that contributes to concentrations observed at the receptor. Footprints can be convolved with emissions inventories and an atmospheric background signal to model tracer concentrations at the receptor, which is the most popular application of the STILT model (Gerbig et al., 2003; Lin et al., 2004; Kort et al., 2008; Macatangay et al., 2008; Miller et al., 2008; Mallia et al., 2015).

This paper discusses limitations within the existing STILT codebase and introduces an updated framework intended to improve the model's applicability to fine-scale spatially distributed measurement approaches. We describe a footprint calculation scheme using a kernel density estimator as well as methods for parallelizing simulations. The value of STILT as a tool for interpreting intracity CO_2 mole fractions is shown using data collected on Salt Lake City's light-rail system. We discuss how results from our analyses can inform future measurement approaches and modeling efforts.

2.2 Modifications to the STILT model

2.2.1 Motivations

The R portion of the STILT model exists as a group of core functions used to track particle locations, calculate footprints, and apply surface flux grids. User groups have built upon these functions, adding wrappers for common modeling workflows and additional functionality. Key components of the higher level functions remain

unpublished, including a description of the footprint calculation. Here, we adopt a widely-used collaborative platform (GitHub) as a common source code repository that meets the needs of the majority of STILT users. This repository is built upon the existing advection and dispersion calculations but has restructured and modernized the core functions used to interact with the model (Figure 2.1). A single script (*run_stilt.r*) defines model inputs such as receptor locations and meteorological fields, controls and executes the parallelized model, and outputs footprints in a NetCDF format consistent with conventions for Climate and Forecast metadata (cfconventions.org). This format is compatible with various data analysis software platforms. Footprints are then convolved with surface flux estimates and an atmospheric background signal to model the tracer concentration at the receptor. *run_stilt.r* serves as the primary interface to the model, interacting with the overhauled higher level functions and providing a systematic, well-documented workflow for users.

STILT was originally intended for applications on regional scales, either modeling mole fraction at the receptor using surface flux inventories or estimating regional scale fluxes based on measured concentrations. Prior to the kernel methods described in the following section, footprints have been calculated by accumulating the influence of particles over an averaging volume. To lessen grid noise from individual particles, the spatial density of the particles was used to dynamically coarsen the size of the averaging volume as the particle cloud spreads, first seen by Gerbig et al. (2003). However, at finer resolutions, this method results in over-smoothing, removing information calculated by the advection and dispersion routines (Figure 2.2).

2.2.2 Description of kernel density estimator

We introduce a kernel density estimator to calculate footprints and show improvements over the traditional method at fine grid resolutions. This method spatially distributes the influence of each particle using a Gaussian weighted kernel centered over the particle's position. The kernel bandwidth is determined at each model time step using elapsed time and dispersion of the stochastic ensemble as proxies for uncertainty in particle locations. Dispersion of the particle cloud is represented using a nondimensionalized standard deviation of particle locations as

$$\sigma = \sqrt{\sigma_x^2 + \sigma_y^2} \tag{2.1}$$

where σ_x^2 and σ_y^2 are the Euclidean variances in horizontal particle positions. We find σ to scale linearly with an average pairwise distance calculation ($r^2 > 0.99$) while operating two orders of magnitude faster. Kernel bandwidths are then calculated as

$$h = S\frac{a\sqrt{t \cdot \sigma}}{\cos\phi}, \tag{2.2}$$

where t is time elapsed in days, $a = 0.06$ is an empirically derived scaling factor, and ϕ is latitude used in an approximation for meridional grid convergence. S is a user-defined smoothing parameter defaulting to $S = 1$, which enables manual manipulation of the kernel sizing to represent unique scenarios.

We test the footprint calculation methods against a simulation with an atypically large particle ensemble size ($N = 100{,}000$) aggregated over a homogeneous grid. This brute force method is computationally expensive but generates an idealized, physically constrained footprint. The simulation receptor was placed at a Salt Lake City CO_2 measurement site on a summertime afternoon and particles were followed backward in time for 24 hours. We then demonstrate differences between the kernel density estimator

and the dynamic grid coarsening footprint calculation methods (Figure 2.2) for a typical particle ensemble ($N = 200$) and for an extreme case with atypically few particles ($N = 10$). The effects of varying the smoothing parameter ($S = 1, 2$) are also shown.

For the standard case ($N = 200$ and $S = 1$), the kernel method shows improved agreement with the brute force method, preserving a near-field Gaussian plume, a clustered area of high influence, and capturing split flow upstream from the receptor. When the kernel bandwidths are doubled by increasing the smoothing parameter ($S = 2$), the footprint field becomes over-smoothed and loses similarity with the brute force case. In the extreme case using atypically few particles ($N = 10$), the dynamic grid coarsening method produces a footprint field dominated by noise from individual particles. The kernel density estimator ($S = 1$) improves results but shows fragmentation further from the receptor. In this case, the scarcity of particles can be compensated for by increasing the smoothing parameter ($S = 2$). While tracer concentration differences between the two footprint calculation methods vary depending upon the locations of footprint differences relative to sources, tracer concentrations calculated using the kernel density estimator show improved similarity with the brute force case.

2.2.3 Model parallelization

Parallelizing simulations is essential to leverage the full capability of computing resources. STILT receptors are defined in a table of x, y, z, t coordinates enabling users to fix a receptor in space and model the time evolution of the influence field, spatially distribute the receptors and capture a snapshot at a single time, or distribute the receptors across both space and time. Since each STILT simulation is computationally

independent, total simulation time can be reduced by distributing batches of simulations between parallel threads. Provided that memory limits are not exceeded, this method enables total simulation time to decrease linearly with available CPU cores. Multinode parallelism is accomplished through interfacing with the Simple Linux Utility for Resource Management (SLURM), an open-source tool that provides the framework for interfacing with clusters of computer nodes. SLURM allocates computational resources with low overhead and can be used to dispatch STILT simulations to multiple nodes. SLURM is used to parallelize *between* nodes and process forking by the modified STILT framework is used to parallelize *within* nodes.

2.3 Evaluation

2.3.1 Salt Lake City light-rail measurements

We demonstrate these changes to STILT by comparing CO_2 mixing ratios simulated by the STILT model with corresponding measurements on-board a Salt Lake City, UT light-rail train during July 2015 (Mitchell et al., 2017). The Salt Lake Valley *km2* area encompassing Salt Lake City and its surrounding suburbs, bounded by the Wasatch mountain range to the east, the Oquirrh mountain range to the west, the Traverse mountain range to the south, and the Great Salt Lake to the northwest. A light-rail train is equipped to measure high-frequency (1 Hz) CO_2 and CH_4 concentrations in repeated transects of the SLV. A Los Gatos Research (LGR) Ultraportable Greenhouse Gas Analyzer performs high-precision CO_2, CH_4 with corrections for water vapor dilution and spectrum broadening. CO_2 and CH_4 mole fractions are calibrated every hour using a reference tank containing compressed air with known tracer concentrations.

Measurements generally show increases in CO_2 mole fraction closer to the urban center and along a north-south oriented urbanized corridor centered in the SLV, consistent with the urban CO_2 "dome" (Idso et al., 2001; Pataki et al., 2007). The lowest concentrations were observed in the southwest corner of the SLV, where suburban development has only recently begun. At a finer scale, the high-frequency measurements show large concentration enhancements near busy roads and intersections. Measured concentrations are also higher along a 3 km section of the light-rail track that runs along the center of a busy six-lane road.

2.3.2 Simulation configuration

STILT simulations are executed over a model domain consisting of a 0.002° grid (roughly 200 m at 41° N) positioned over the SLV. Light-rail measurements are averaged hourly over this grid and STILT receptors placed at the center of cells containing measurements. This grid resolution and timescale for the month of July, 2015 results in 31,964 unique receptors, necessitating the use of parallelized simulations and fine-scale footprint calculation included in the modified framework. The experimental High Resolution Rapid Refresh (HRRR) mesoscale meteorological model is used to drive 24 h backward simulations of 200 particles for each receptor. These simulations completed in just under 18 hours utilizing 40 parallel threads across 5 nodes, each equipped with 64 GB of memory with two 8-core Intel XEON E5-2670 2.6 GHz processors. Footprints are then convolved with anthropogenic and biological CO_2 flux estimates and added to background CO_2 observations from a nearby high-elevation measurement site at Hidden Peak, as part of Snowbird ski resort in the Wasatch Mountains (Stephens et al., 2011).

We focus on observations collected during afternoon and evening hours (13:00-20:00 LDT) to lessen the influence of boundary layer development and shallow turbulence on measured concentrations that would not be represented in the 3 km resolution of the HRRR meteorology.

2.3.3 Emissions inventories

The Hestia bottom-up anthropogenic CO_2 emissions inventory characterizes carbon fluxes by estimating emissions at the scale of individual buildings and roadways (Gurney et al., 2012). Hestia is available for a handful of U.S. cities including Indianapolis, Los Angeles, Baltimore/D.C., and Salt Lake City. Details pertaining to the Salt Lake City Hestia product are described by Patarasuk et al. (2016). These anthropogenic CO_2 flux estimates are aggregated hourly to 0.002° (Figure 2.3). The biological inventory determines surface types using the 2011 National Land Cover Database (Homer et al., 2007) with 1 m LIDAR derived discrete land cover classifications over the SLV (Catharine et al., 2017). An eddy covariance-based lookup table is used to estimate biological fluxes based on land cover classifications over a 0.01° grid. The biological inventory is bilinearly interpolated to the 0.002° grid.

2.3.4 Results

The model captured the concentration gradient between the urban center and surrounding suburbs (Figure 2.4). Lowest modeled concentrations occurred in the southwest corner of the SLV in agreement with measurements. The model also reproduced concentration enhancements downwind from major roadways as well as

captured the evening rush hour enhancement (Figure 2.5). On average, we found the ($\Delta CO2 = -1.0\ ppm$) to be 80% lower than the anthropogenic contribution ($\Delta CO2 = 5.1\ m$).

Key differences between modeled and measured concentrations exist near hyper-local sources at the sub-grid scale (Figure 2.4). While the model does capture localized concentration enhancements near busy roads, measured concentrations are systematically higher than corresponding model estimates in these areas. These results indicate that the light-rail platform is directly sampling emissions before they become adequately mixed with the surrounding air. This is also evident for the section of light-rail track that runs along the center of a busy road. The model, distributing sub-grid scale emissions throughout the grid cell, shows some localized enhancement but does not fully capture the magnitude of concentration enhancement resulting from direct sampling of the emissions source.

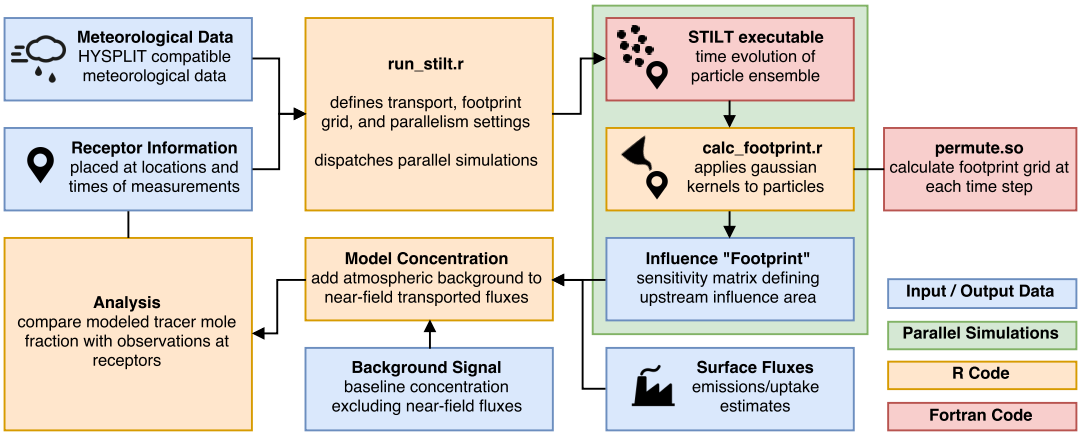

Figure 2.1. STILT workflow to model tracer concentrations at a receptor. STILT advects particles and calculates the influence footprint for each receptor. Footprints are convolved with surface fluxes and an atmospheric background signal to model the tracer concentrations.

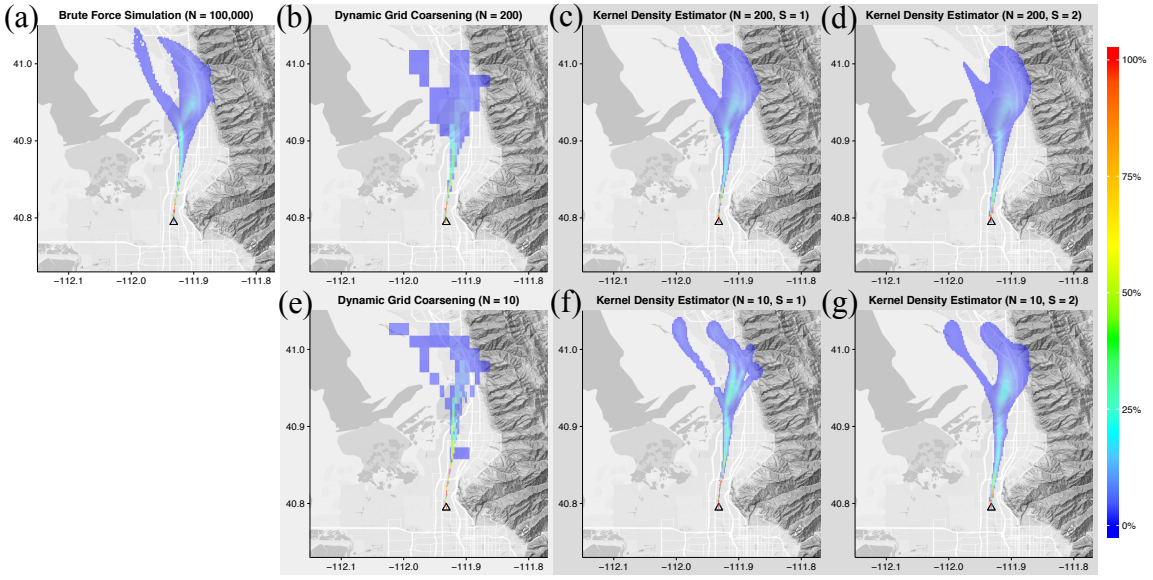

Figure 2.2. Comparison of footprint calculation methods. Simulating a large number of particles and gridding by location (a) gives a physically constrained expectation for the footprint. Using subsets of 200 particles (b-d) and 10 particles (e-g), the kernel density estimator demonstrates considerable improvements over the traditional dynamic grid coarsening. Modifying the kernel bandwidths ($\boldsymbol{S = 2}$) can improve results in uncommon cases, such as the 10 particle ensemble case (g).

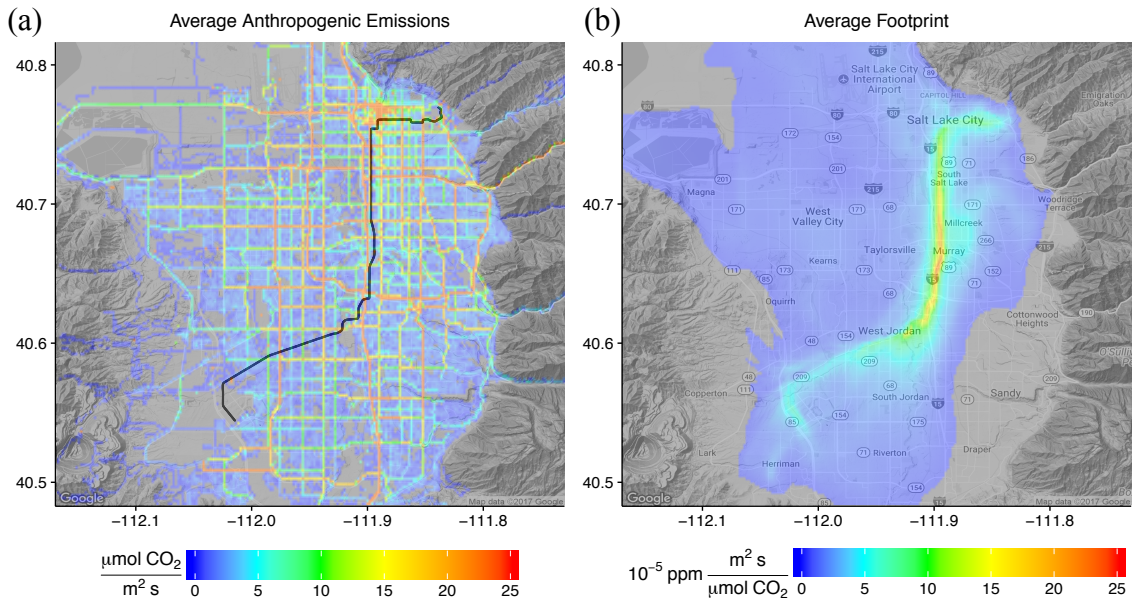

Figure 2.3. July 2015 average anthropogenic emissions (a) overlaid with light-rail route and average modeled footprint observed by light-rail (b). The anthropogenic and biospheric flux inventories convolved with the footprints give the contribution of near-field fluxes to measured concentrations in ppm.

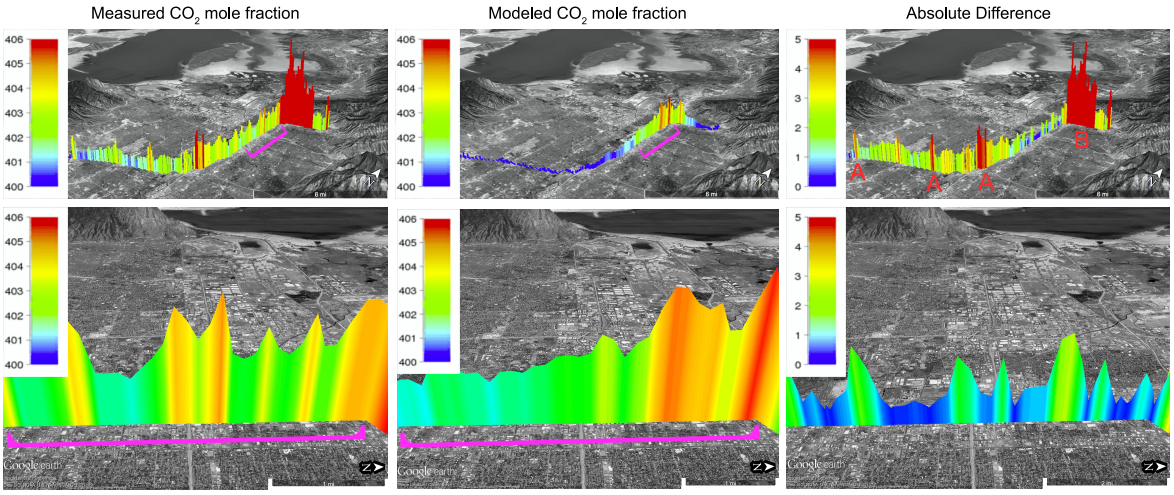

Figure 2.4. Key differences between measured and modeled tracer mole fraction occur near hyper-local sources, including passing large roadways (A) and where the light-rail track is shared by other vehicles on the roadway (B). The model captures the overall urban-suburban-rural CO_2 gradient as well as localized enhancements near busy roads.

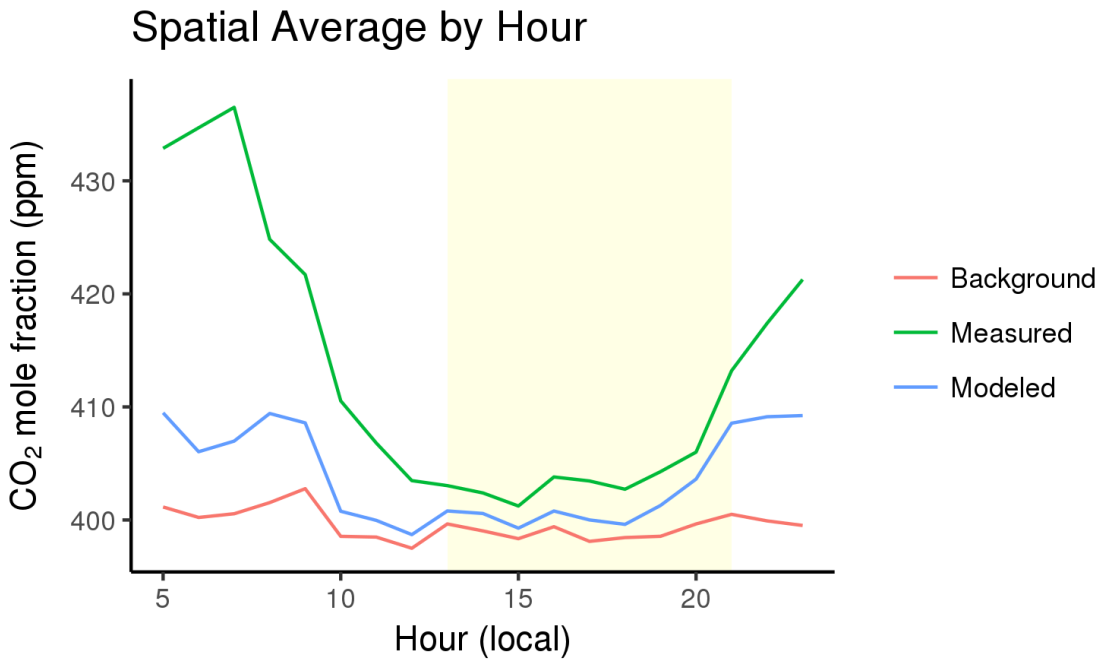

Figure 2.5. Spatially averaged mole fraction for light-rail operating hours from early morning to late evening. Yellow indicates hours used for spatial comparisons. Modeled concentrations agree well with measurements, with underestimation caused by sub-grid scale sampling of emissions sources.

CHAPTER 3

CONCLUSION

We have introduced modifications to the STILT model that address prior limitations. These changes enable the STILT model to be a key tool for investigating fine-scale patterns in urban emissions. Given the importance of footprints in the STILT workflow, a kernel density estimator was applied and shown to improve agreement with an idealized brute force method. High level methods for single and multinode parallelism were incorporated into this distribution, significantly reducing total simulation times. We then applied STILT to model CO_2 mole fractions for a Salt Lake City light-rail train at a 0.002° resolution and show that the model and observations agree on average spatial and temporal patterns during the afternoon period, with key differences occurring in the proximity of sub-grid scale sources.

Results indicate fine-scale inverse analyses will show a high sensitivity to measurement-source proximity. Observation techniques striving to quantify fine-scale emissions or assess the validity of emissions inventories should seek to reduce the influence of hyper-local sources. Prioritizing measurement placement at the top of large buildings or at least 0.5 km from large sources such as busy roadways enables dispersion of pollutants and reduces direct sampling of emissions. Modeling techniques seeking to utilize platforms subject to large sources at the sub-grid scale should strive to develop a

mechanism to describe and account for the sampling of emissions prior to adequate mixing.

Future direction includes further model modifications, including merging STILT-R version 2 with recent changes to the HYSPLIT model. To take full advantage of modern technologies, improvements described in Chapter 2 will be combined with updates to HYSPLIT's mean trajectory calculation. This tool will then be applied to measurements made on the light-rail train over a longer timescale, as well as to the Nerdmobile mobile laboratory and stationary measurement sites distributed throughout Northern Utah.

REFERENCES

Apte, J. S., and Coauthors, 2017: High-resolution air pollution mapping with Google street wiew cars: Exploiting big data. *Environ. Sci. Technol.*, **51**, 6999–7008, doi:10.1021/acs.est.7b00891.

Briber, B., L. Hutyra, A. Dunn, S. Raciti, and J. Munger, 2013: Variations in atmospheric CO_2 mixing ratios across a Boston, MA urban to rural gradient. *Land*, **2**, 304–327, doi:10.3390/land2030304. http://www.mdpi.com/2073-445X/2/3/304/.

Bush, S. E., F. M. Hopkins, J. T. Randerson, C.-T. T. Lai, and J. R. Ehleringer, 2015: Design and application of a mobile ground-based observatory for continuous measurements of atmospheric trace gas and criteria pollutant species. *Atmos. Meas. Tech.*, **8**, 33–63, doi:10.5194/amtd-8-33-2015. http://www.atmos-meas-tech-discuss.net/8/33/2015/amtd-8-33-2015.html (Accessed May 25, 2015).

Canadell, J. G., and Coauthors, 2007: Contributions to accelerating atmospheric CO_2 growth from economic activity, carbon intensity, and efficiency of natural sinks. *Proc. Natl. Acad. Sci. U. S. A.*, **104**, 18866–18870, doi:10.1073/pnas.0702737104. http://www.scopus.com/inward/record.url?eid=2-s2.0-36749099520&partnerID=tZOtx3y1.

Catharine, D., C. Strong, J. C. Lin, A. Chekov, D. Mendoza, L. Mitchell, and P. Dennison, manuscript in preparation: A multiple-box atmospheric inverse model: observationally guided estimates of surface carbon dioxide emissions in Northern Utah.

Christen, A., 2014: Atmospheric measurement techniques to quantify greenhouse gas emissions from cities. *Urban Clim.*, **10**, 1–20, doi:10.1016/j.uclim.2014.04.006. http://linkinghub.elsevier.com/retrieve/pii/S2212095514000327.

Clark, L. P., D. B. Millet, and J. D. Marshall, 2014: National patterns in environmental injustice and inequality: Outdoor NO_2 air pollution in the United States. *PLoS One*, **9**, e94431, doi:10.1371/journal.pone.0094431. http://dx.doi.org/10.1371/journal.pone.0094431 (Accessed May 12, 2015).

Duren, R. M., and C. E. Miller, 2012: Measuring the carbon emissions of megacities. *Nat. Clim. Chang.*, **2**, 560–562. http://dx.doi.org/10.1038/nclimate1629.

Gately, C. K., L. R. Hutyra, and I. Sue Wing, 2015: Cities, traffic, and CO_2 : A multidecadal assessment of trends, drivers, and scaling relationships. *Proc. Natl. Acad. Sci.*, **112**, 4999–5004, doi:10.1073/pnas.1421723112. http://www.pnas.org/lookup/doi/10.1073/pnas.1421723112.

Gerbig, C., J. C. Lin, S. C. Wofsy, B. C. Daube, A. E. Andrews, B. B. Stephens, P. S. Bakwin, and C. A. Grainger, 2003: Toward constraining regional-scale fluxes of CO_2 with atmospheric observations over a continent: 2. Analysis of COBRA data using a receptor-oriented framework. *J. Geophys. Res. Atmos.*, doi:10.1029/2003JD003770.

Gurney, K. R., I. Razlivanov, Y. Song, Y. Zhou, B. Benes, and M. Abdul-Massih, 2012: Quantification of fossil fuel CO_2 emissions on the building/street scale for a large U.S. city. *Environ. Sci. Technol.*, **46**, 12194–12202, doi:10.1021/es3011282. http://dx.doi.org/10.1021/es3011282.

Gurney, K. R., and Coauthors, 2015: Track urban emissions on a human scale. *Nature*, **525**, 179–181, doi:10.1038/525179a. http://www.nature.com/news/climate-change-track-urban-emissions-on-a-human-scale-1.18311.

Homer, C., and Coauthors, 2007: Completion of the 2001 National Land Cover Database for the Conterminous United States. *Photogramm. Eng. Remote Sens.*, **73**, 337–341, doi:citeulike-article-id:4035881.

Hoornweg, D., Freire, M., Lee, M. J. Bhada-Tata, P., and Yuen, B., 2011: *Cities and climate change: responding to an urgent agenda*. The World Bank, 306 pp. https://doi.org/10.1596/978-0-8213-8493-0.

Hopkins, F. M., E. A. Kort, S. E. Bush, J. R. Ehleringer, C.-T. Lai, D. R. Blake, and J. T. Randerson, 2016: Spatial patterns and source attribution of urban methane in the Los Angeles Basin. *J. Geophys. Res. Atmos.*, doi:10.1002/2015JD024429.

Idso, C. D., S. B. Idso, and R. C. Balling Jr., 2001: An intensive two-week study of an urban CO_2 dome in Phoenix, Arizona, USA. *Atmos. Environ.*, **35**, 995–1000, doi:10.1016/S1352-2310(00)00412-X. http://www.sciencedirect.com/science/article/pii/S135223100000412X%5Cnhttp://www.sciencedirect.com/science?_ob=MiamiImageURL&_cid=271798&_user=2139759&_pii=S135223100000412X&_check=y&_origin=&_coverDate=31-Dec-2001&view=c&wchp=dGLzVlt-zSkWz&md5=bf829efbf143.

Jackson, R. B., A. Down, N. G. Phillips, R. C. Ackley, C. W. Cook, D. L. Plata, and K. Zhao, 2014: Natural gas pipeline leaks across Washington, DC. *Environ. Sci. Technol.*, doi:10.1021/es404474x.

Kennedy, C., and Coauthors, 2009: Greenhouse gas emissions from global cities. *Environ. Sci. Technol.*, **43**, 7297–7302, doi:10.1021/es900213p.

Kort, E. A., and Coauthors, 2008: Emissions of CH_4 and N_2O over the United States and Canada based on a receptor-oriented modeling framework and COBRA-NA atmospheric observations. *Geophys. Res. Lett.*, **35**, 1–5, doi:10.1029/2008GL034031.

Lee, J. K., A. Christen, R. Ketler, and Z. Nesic, 2017: A mobile sensor network to map carbon dioxide emissions in urban environments. *Atmos. Meas. Tech.*, **10**, 645–665, doi:10.5194/amt-10-645-2017.

Lin, J. C., and C. Gerbig, 2005: Accounting for the effect of transport errors on tracer inversions. *Geophys. Res. Lett.*, **32**, 1–5, doi:10.1029/2004GL021127.

Lin, J. C., C. Gerbig, S. C. Wofsy, A. E. Andrews, B. C. Daube, K. J. Davis, and C. A. Grainger, 2003: A near-field tool for simulating the upstream influence of atmospheric observations: The Stochastic Time-Inverted Lagrangian Transport (STILT) model. *J. Geophys. Res.*, **108**, ACH 2-1-ACH 2-17, doi:10.1029/2002JD003161.

Lin, J. C., and Coauthors, 2004: Measuring fluxes of trace gases at regional scales by Lagrangian observations: Application to the CO_2 Budget and Rectification Airborne (COBRA) study. *J. Geophys. Res. D Atmos.*, **109**, 1–23, doi:10.1029/2004JD004754.

Macatangay, R., T. Warneke, C. Gerbig, S. Körner, R. Ahmadov, M. Heimann, and J. Notholt, 2008: A framework for comparing remotely sensed and in-situ CO_2 concentrations. *Atmos. Chem. Phys.*, **8**, 2555–2568, doi:10.5194/acp-8-2555-2008. http://www.scopus.com/inward/record.url?eid=2-s2.0-43849111352&partnerID=tZOtx3y1.

Mallia, D. V, J. C. Lin, S. Urbanski, J. Ehleringer, and T. Nehrkorn, 2015: Impacts of upstream wildfire emissions on CO , CO_2 , and $PM_{2.5}$ concentrations in Salt Lake City , Utah. *J. Geophys. Res. Atmos.*, **120**, 147–166, doi:10.1002/2014JD022472.

Marchese, A. J., and Coauthors, 2015: Methane emissions from United States natural gas gathering and processing. *Environ. Sci. Technol.*, doi:10.1021/acs.est.5b02275.

Mays, K. L., P. B. Shepson, B. H. Stirm, A. Karion, C. Sweeney, and K. R. Gurney, 2009: Aircraft-based measurements of the carbon footprint of Indianapolis. *Environ. Sci. Technol.*, **43**, 7816–7823, doi:10.1021/es901326b.

McKain, K., and Coauthors, 2015: Methane emissions from natural gas infrastructure and use in the urban region of Boston, Massachusetts. *Proc. Natl. Acad. Sci. U. S. A.*, **112**, 1941–1946, doi:10.1073/pnas.1416261112. http://www.pnas.org/content/112/7/1941.short.

McKain, K., S. C. Wofsy, T. Nehrkorn, J. Eluszkiewicz, J. R. Ehleringer, and B. B. Stephens, 2012: Assessment of ground-based atmospheric observations for verification of greenhouse gas emissions from an urban region. *Proc. Natl. Acad. Sci. U. S. A.*, **109**, 8423–8428, doi:10.1073/pnas.1116645109. http://www.pnas.org/cgi/content/long/109/22/8423 (Accessed May 26, 2015).

Meure, C. M., D. Etheridge, C. Trudinger, P. Steele, R. Langenfelds, T. Van Ommen, A. Smith, and J. Elkins, 2006: Law Dome CO_2, CH_4 and N_2O ice core records extended to 2000 years BP. *Geophys. Res. Lett*, **33**, doi:10.1029/.

Miller, S. M., and Coauthors, 2008: Sources of carbon monoxide and formaldehyde in North America determined from high-resolution atmospheric data. *Atmos. Chem. Phys.*, **8**, 7673–7696, doi:10.5194/acp-8-7673-2008. http://www.atmos-chem-phys.net/8/7673/2008/.

Mitchell, L., and Coauthors, manuscript in preparation: Continuous monitoring of trace gases and pollutants using a light rail public transit platform.

Nehrkorn, T., J. Eluszkiewicz, S. C. Wofsy, J. C. Lin, C. Gerbig, M. Longo, and S. Freitas, 2010: Coupled weather research and forecasting-stochastic time-inverted lagrangian transport (WRF-STILT) model. *Meteorol. Atmos. Phys.*, **107**, 51–64, doi:10.1007/s00703-010-0068-x.

Newman, S., X. Xu, H. P. Affek, E. Stolper, and S. Epstein, 2008: Changes in mixing ratio and isotopic composition of CO_2 in urban air from the Los Angeles basin, California, between 1972 and 2003. *J. Geophys. Res.*, **113**, D23304, doi:10.1029/2008JD009999. http://doi.wiley.com/10.1029/2008JD009999.

Pataki, D. E., T. Xu, Y. Q. Luo, and J. R. Ehleringer, 2007: Inferring biogenic and anthropogenic carbon dioxide sources across an urban to rural gradient. *Oecologia*, **152**, 307–322, doi:10.1007/s00442-006-0656-0.

Patarasuk, R., and Coauthors, 2016: Urban high-resolution fossil fuel CO_2 emissions quantification and exploration of emission drivers for potential policy applications. *Urban Ecosyst.*, **19**, 1013–1039, doi:10.1007/s11252-016-0553-1.

Phillips, N. G., and Coauthors, 2013: Mapping urban pipeline leaks: Methane leaks across Boston. *Environ. Pollut.*, doi:10.1016/j.envpol.2012.11.003.

Ramamurthy, P., and E. R. Pardyjak, 2011: Toward understanding the behavior of carbon dioxide and surface energy fluxes in the urbanized semi-arid Salt Lake Valley, Utah, USA. *Atmos. Environ.*, **45**, 73–84, doi:10.1016/j.atmosenv.2010.09.049. http://linkinghub.elsevier.com/retrieve/pii/S1352231010008356.

Raupach, M. R., and J. G. Canadell, 2010: Carbon and the Anthropocene. *Curr. Opin. Environ. Sustain.*, **2**, 210–218, doi:10.1016/j.cosust.2010.04.003. http://dx.doi.org/10.1016/j.cosust.2010.04.003.

Schmidt, A., C. W. Rella, M. G??ckede, C. Hanson, Z. Yang, and B. E. Law, 2014: Removing traffic emissions from CO2 time series measured at a tall tower using mobile measurements and transport modeling. *Atmos. Environ.*, **97**, 94–108, doi:10.1016/j.atmosenv.2014.08.006.

Seto, K. C., B. Güneralp, and L. R. Hutyra, 2012: Global forecasts of urban expansion to 2030 and direct impacts on biodiversity and carbon pools. *Proc. Natl. Acad. Sci. U. S. A.*, **109**, 16083–16088, doi:10.1073/pnas.1211658109. http://www.pnas.org/content/109/40/16083.abstract.

Shusterman, A. A., V. Teige, A. J. Turner, C. Newman, J. Kim, and R. C. Cohen, 2016: The BErkeley Atmospheric CO_2 Observation Network: initial evaluation. *Atmos. Chem. Phys. Discuss.*, 1–23, doi:10.5194/acp-2016-530. http://www.atmos-chem-phys-discuss.net/acp-2016-530/.

Stein, A. F., R. R. Draxler, G. D. Rolph, B. J. B. Stunder, M. D. Cohen, and F. Ngan, 2015: NOAA's HYSPLIT Atmospheric Transport and Dispersion Modeling System. *Bull. Am. Meteorol. Soc.*, **96**, 2059–2077, doi:10.1175/BAMS-D-14-00110.1.

Stephens, B. B., N. L. Miles, S. J. Richardson, A. S. Watt, and K. J. Davis, 2011: Atmospheric CO_2 monitoring with single-cell NDIR-based analyzers. *Atmos. Meas. Tech.*, **4**, 2737–2748, doi:10.5194/amt-4-2737-2011.

Stohl, a., C. Forster, A. Frank, P. Seibert, and G. Wotawa, 2005: Technical note: The Lagrangian particle dispersion model FLEXPART version 6.2. *Atmos. Chem. Phys. Discuss.*, **5**, 4739–4799, doi:10.5194/acpd-5-4739-2005.

Sun, J., and Coauthors, 2014: Use of NWP for nowcasting convective precipitation: Recent progress and challenges. *Bull. Am. Meteorol. Soc.*, **95**, 409–426, doi:10.1175/BAMS-D-11-00263.1.

Taylor, G. I., 1922: Diffusion by continuous movements. *Proc. London Math. Soc.*, **s2-20**, 196–212, doi:10.1112/plms/s2-20.1.196.

Turnbull, J. C., and Coauthors, 2015: Toward quantification and source sector identification of fossil fuel CO_2 emissions from an urban area: Results from the INFLUX experiment. *J. Geophys. Res. Atmos.*, **120**, 292–312, doi:10.1002/2014JD022555. http://doi.wiley.com/10.1002/2014JD022555 (Accessed December 18, 2015).

U.S. EPA, C. C. D., 2016: Inventory of U.S. Greenhouse Gas Emissions and Sinks : 1990 – 2014. https://www3.epa.gov/climatechange/ghgemissions/usinventoryreport.html.

US EPA, C. C. D., 2015: Methane Emissions. http://www3.epa.gov/climatechange/ghgemissions/gases/ch4.html.

Vogelezang, D. H. P., and A. A. M. Holtslag, 1996: Evaluation and model impacts of alternative boundary-layer height formulations. *Boundary-Layer Meteorol.*, **81**, 245–269, doi:10.1007/BF02430331.

Wallace, J. M., and P. V. Hobbs, 2006: *Atmospheric Science: An Introductory Survey: Second Edition*. 1-488 pp.

Wentz, E. A., P. Gober, R. C. Balling, and T. A. Day, 2002: Spatial patterns and determinants of winter atmospheric carbon dioxide concentrations in an urban environment. *Ann. Assoc. Am. Geogr.*, **92**, 15–28.

Wolff, E. W., 2011: Global change: Methane and monsoons. *Nature*, **470**, doi:10.1038/470049a.